Exploration Geophysics

ISSN: 0812-3985 (Print) 1834-7533 (Online) Journal homepage: https://www.tandfonline.com/loi/texg20

On airborne IP effects in standard AEM systems: tightening model space with data space

Andrea Viezzoli & Giovanni Manca

To cite this article: Andrea Viezzoli & Giovanni Manca (2019): On airborne IP effects in standard AEM systems: tightening model space with data space, Exploration Geophysics, DOI: 10.1080/08123985.2019.1681895

To link to this article: https://doi.org/10.1080/08123985.2019.1681895

Published online: 06 Nov 2019.

Submit your article to this journal

Article views: 44

View related articles

View Crossmark data

Full Terms & Conditions of access and use can be found at
https://www.tandfonline.com/action/journalInformation?journalCode=texg20

EXPLORATION GEOPHYSICS
https://doi.org/10.1080/08123985.2019.1681895

Taylor & Francis
Taylor & Francis Group

Check for updates

On airborne IP effects in standard AEM systems: tightening model space with data space

Andrea Viezzoli[a] and Giovanni Manca[b]

[a]Aarhus Geophysics Aps, Risskov, Denmark; [b]Aarhus Geofisica Srl, Pisa, Italy

ABSTRACT
IP effects in AEM data are subject of current research around the world. There have been success stories and it is now practical to model AIP. It is widely accepted that failure to account for IP effects, when present, will produce artefacts in the resistivity model. However there still is a need to study more accurately the boundaries of the effect on AEM data and of its relevance, beyond common past acceptance. This paper provides a clear and extensive overview of detectable AIP effects in the data space, without imposing simplistic assumptions (e.g. fixing some parameters to arbitrary values or limited boundaries), beside using a 1D approach. We produce forward responses with dispersive resistivity for hundreds of thousands of combinations of Cole–Cole model parameters (different rock types) and AEM system transfer functions. The results are analysed using various metrics (e.g. sum of negative voltages, exponential fitting), presented with a series of 3D plots that capture different AIP signatures in the transients. Experiments include half spaces, 2 and 3 layer models, combined with different waveforms, Rx types (dB/dt and B), Tx-Rx geometries, flying heights, base frequencies. The results allow a clear assessment of the different aspects of AIP effects over a wide range of geological and geophysical situations. Measured AIP effects are mostly focused in the range of τ from 10^{-2} s to 10^{-4} s. Measurable AIP effects depend on AEM system's specs, are often unpredictable, can originate from chargeable layers at considerable depth, are heavily affected by layering and can occur over a wide range of situations. Deeper chargeable layers do not necessarily produce fainter AIP anomalies. What can be generalised is that AIP effects are increased most often by the presence of a resistive bedrock, often using slow turn-off of the waveform, are generally better observed with B field instead of dB/dt and lowering base frequencies. They can vary abruptly, due to the rapidly changing relative contribution of pure EM and pure IP responses. AIP effects can occur more often than previously thought and should not be discarded a-priori from any AEM survey.

ARTICLE HISTORY
Received 4 September 2018
Accepted 15 July 2019

KEYWORDS
3D modelling; airborne electromagnetics; case histories; exploration methodologies; mineral exploration; interpretation

Introduction

Induced polarisation effects on airborne electromagnetic data (AIP) have been identified for some time now (Smith and West 1988; Flis, Newman, and Hohmann 1989; Smith 1989; Smith and Klein 1996). AIP effects are easier to detect in the coincident-loop, high-powered, better signal/noise more recently developed systems. There are several different locations (e.g. Australia, Canada, Scandinavia, and Central Africa) where AIP have been frequently reported and recorded. At these locations the presence of chargeable material can be associated with material such as permafrost, lake sediments, weathered regolith and local mineralisation alterations, which in some cases, can also produce measurable AIP effects. It is by now also accepted that failure to account for IP effects, when present, will produce artefacts in the resistivity models. One of the fundamental questions that still remains open in the industry is how much IP effect is present in "standard" AEM systems' data.

Recent studies are pushing the AIP boundaries (e.g. Chen, Hodges, Smiarowski 2015; Kang, Fournier, and Oldenburg 2017; Viezzoli, Kaminski, and Fiandaca 2017) although still often posing somewhat restricting assumptions on parameters (e.g. Oldenburg and Kang 2015; Macnae 2016; Kang, Fournier, and Oldenburg 2017 fix c to a predefined value) or modelling approach (e.g. thin sheet). Beside considerations about which is the best model (e.g. other than single Cole Cole, e.g. Fiandaca et al. 2012; Kratzer and Macnae 2012) to describe IP in AEM, some of the restrictions applied arise also from the understandable desire to reduce parameters that we solve for, or CPU time. They might however prevent us from seeing the full picture. Conclusions about IP effects being at all present in the AEM data should be drawn on as unbiased assumptions as possible, and not on what could be later possibly recovered by further modelling/inversion.

There is therefore a need to study more systematically the actual general boundaries of the effect and of its relevance, starting from the data space. This paper aims at providing a robust contribution to this topic. It studies thoroughly the correlation between parameters and data, using simple synthetic 1D AIP modelling of different nominal AEM systems, in presence of different

CONTACT Giovanni Manca Giovanni.manca@aarhusgeo.com Aarhus Geofisica Srl, Pisa 56023, Italy

© 2019 Australian Society of Exploration Geophysics

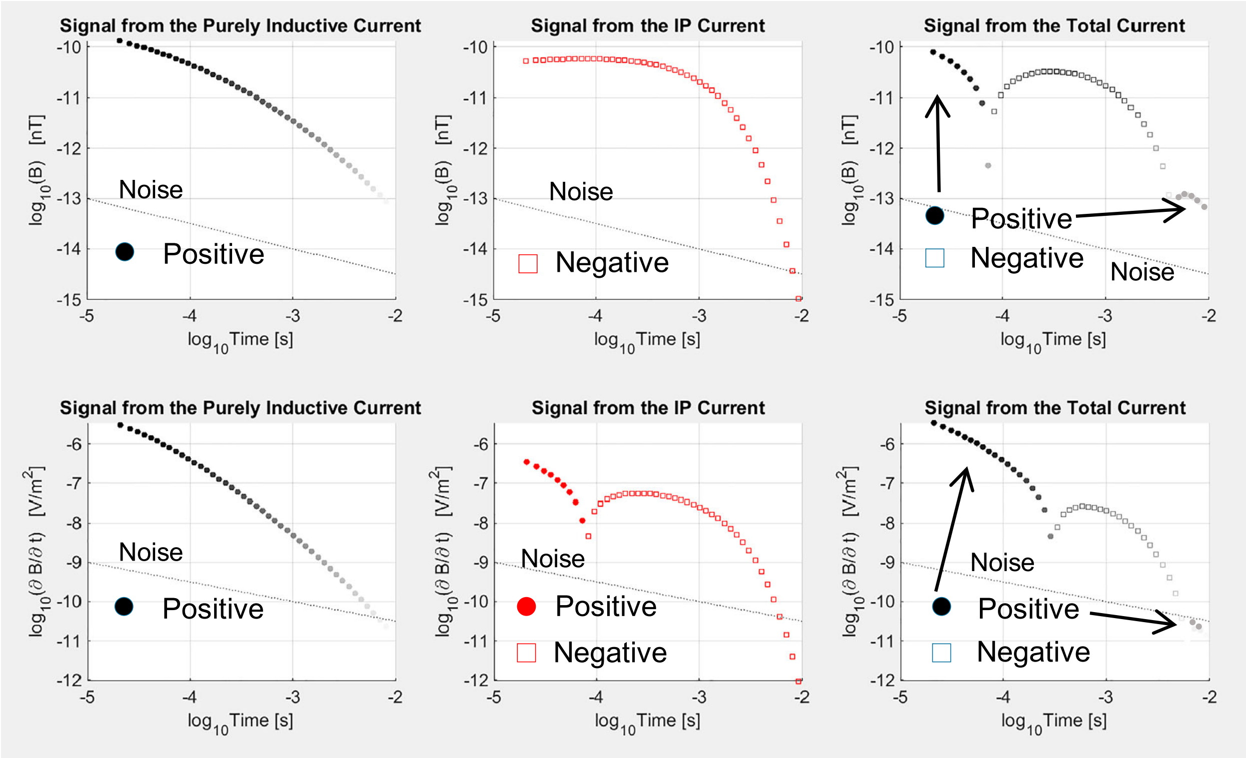

Figure 1. Synthetic response of a VTEM-like AEM system (right column, B receiver at top, dB/dT at bottom) over a 3 layer model (first chargeable), showing the relative contribution of pure EM currents (left column) and of IP currents (central column).

simplified geologies. We chase this goal starting from illustrative display and analysis of individual transients associated with 1D models. Then we quickly move to different IP-related metrics displayed in 3D plots that group the results, allowing a generalisation of the findings.

Before describing in more details the methodology applied, it is useful to briefly recap the main physical principles of the AIP effect, drawing from earlier work (e.g. Flis, Newman, and Hohmann 1989; Smith 1989). The industry calls AIP the effects of the dispersive nature of resistivity (conductivity), which can manifest themselves in the frequency range of AEM systems. This range's boundaries are limited by the base frequency of the system, the duration of the ramp down, eventual hardware or digital filters. Standard AEM systems (25 Hz) therefore focus their range between 10^1 and 10^5 Hz. Newer system are pushing the lower boundary, lowering base frequencies to 12.5 Hz, 6.25, and even 3.125 (Macnae 2017). Even with lowering base frequencies, AEM's sensitivity remains centred in the $\sim [10^{-2}: 10^{-4}]$ Hz range, orders of magnitudes above the usual sub-Hz frequencies of ground IP surveys mostly deployed in mineral exploration (Macnae 2016). As a consequence of the frequency range, the IP effects measured in standard AEM are likely associated to fine grained materials, alteration zones, permafrost.

As well known, during current ramp down, the time varying primary field induces an electromagnetic force. Charge carriers respond to the EMF with Cole Cole time

Table 1. Model parameters associated with the responses at Figure 1.

	RHO (ohm.m)	M (mV/V)	TAU (seconds)	C (number)	THK (metres)
Layer 1	100	300	10^{-3}	0.5	30
Layer 2	500	0	NA	NA	100
Layer 3	10	0	NA	NA	infinite

constants τ ranging from 10^{-1} to 10^{-5} s, with the resulting current charging the ground up. After end of ramp down, they start discharging, creating an "IP" current, which adds up to the standard "pure EM" eddy currents. Both IP and EM currents decay over time, but have opposite direction. The first are restricted to the chargeable material(s), the second have a peak value that travel downward. The AEM receiver measures the time varying flux of the total secondary magnetic field, made of the vector sum of the secondary fields associated to IP and EM currents. Figure 1 shows the different contributions of currents to the measured responses (for a VTEM-like system) of a B and a dB/dt receiver over a simple layered earth with a shallow chargeable unit and a deep conductor (could be a conductive basement). Table 1 reports the details of the models parameters. Notice how the IP current (middle column) dominate the total measured response (right column) from very early on. The "conductive basement's" response starts showing at very late times, just above noise for the B receiver, and below noise for the dB/dt. Compare with the response from a non-chargeable ground in the left column.

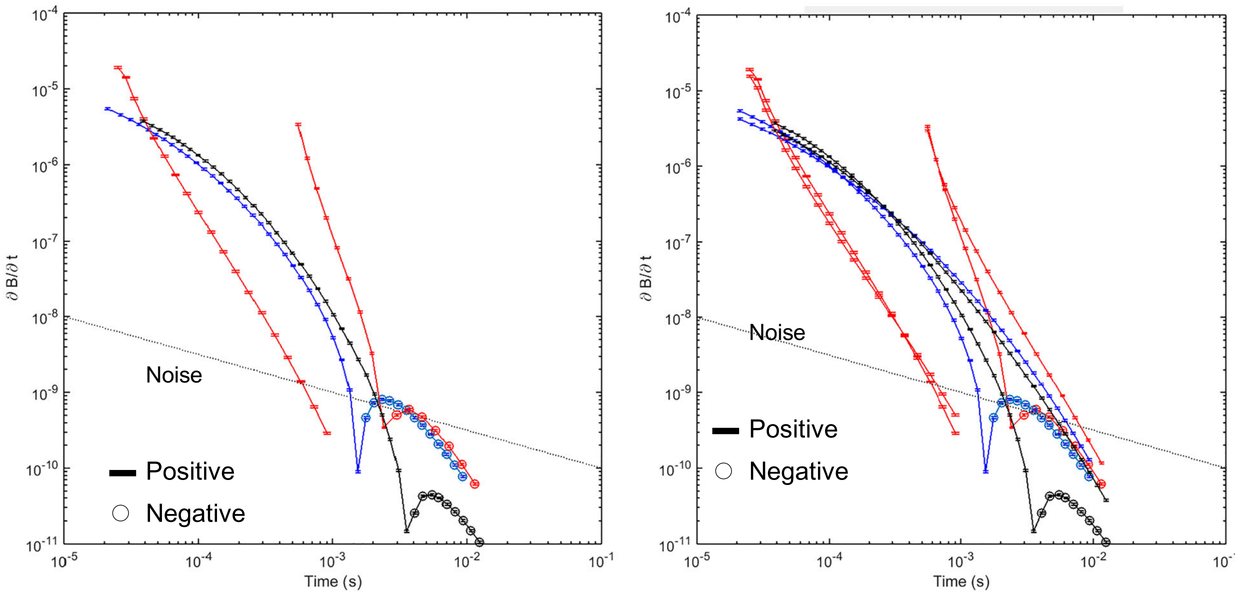

Figure 2. FWD response of different AEM systems (VTEM = blue, SkyTEM = red, Xcite = black), over a polarizable homogeneous half space with $\rho = 200\ \Omega$m, m = 300 mV/V, τ = 1 ms, $c = 0.5$. Solid symbols represents positive voltages, empty circles negative voltages, the dashed lines typical noise level.

A final introductory note, for exploration, about the probable source of AIP effects mentioned above. Although arguably not suitable for direct mapping of economic deposits of disseminated sulphides, AIP can inform about fine grained related sources, possibly related to alterations. Also, ignoring IP effects in AEM will produce severely erroneous resistivities models. In any case, more fundamental research is required to fully assess the sources of the AIP effects and their relevance in different geologies and exploration models.

Methods and results

The FWD responses of layered earth with IP (we use the dispersive Cole Cole model, with low frequency resistivity limit) are obtained with AarhusInv (Fiandaca et al. 2012), for different systems and different layering of electrical properties. Figure 2 shows the AIP effect in responses (V/m^2) of different AEM systems over a homogeneous half space, both chargeable (left) and non-chargeable (right). It is obvious that IP affects transients in different ways, depending on system's specs. In this case, the main difference between these responses is due to relevance of the duration of the ramp down (SkyTEM being the fastest, VTEM the slowest), as discussed in the introduction.

Calculating few tens of forward responses with varying combinations of Cole Cole parameters is enough to immediately realise how the IP effects can combine in dramatic and often unpredictable ways in the data space. See for example Figure 3, in which we slightly changed values of the Cole Cole parameters of the homogenous half space with respect to the responses in the previous figure.

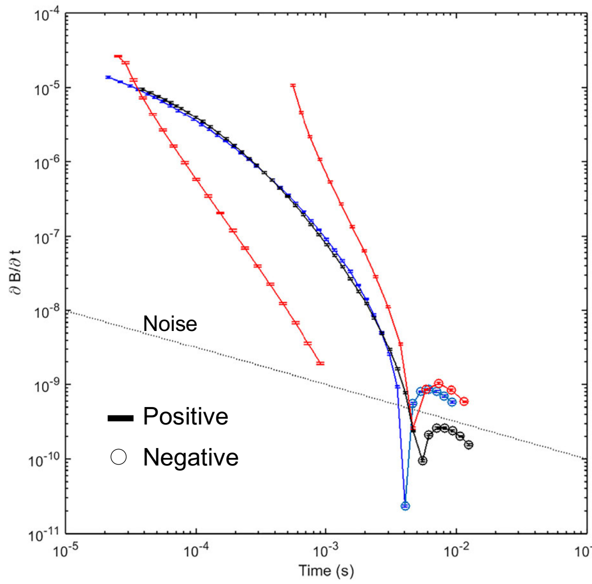

Figure 3. FWD response of different AEM systems (VTEM = blue, SkyTEM = red, Xcite = black), over a polarizable homogeneous half space with $\rho = 100\ \Omega$m, m = 300 mV/V, τ = 10 ms, $c = 0.7$. Solid symbols represents positive voltages, empty circles negative voltages, the dashed lines typical noise level. Compare against Figure 2.

Applying small variations to each of the Cole Cole parameters in the proximity of the combinations shown in Figures 2 and 3 would yield a suite of continuously changing responses, sometimes with rather abrupt variations. Often the transients get distorted by IP without ever giving a measurable change in sign.

Things get even more varied when dealing with a layered earth rather than homogenous half space. Figure 4 shows the response of the AEM systems over a 2 layer

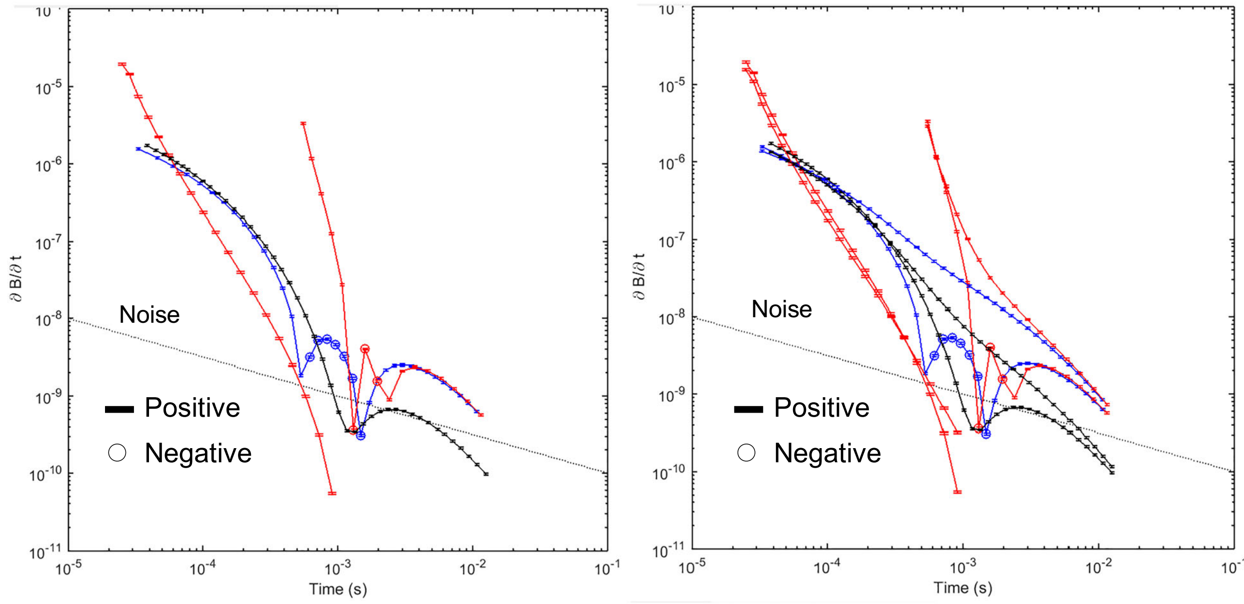

Figure 4. FWD response of different AEM systems (VTEM = blue, SkyTEM = red, Xcite = black), over a 2 layered model. The first layer, 400 m thick, is polarizable homogeneous with $\rho = 200\ \Omega$m, m = 300 mV/V, $\tau = 1$ ms, c = 0.5 (same as for the homogenous half space of Figure 2). The second layer is conductive (10 Ωm) and non-chargeable. Solid symbols represents positive voltages, empty circles negative voltages, the dashed lines typical noise level.

model, in which we added a second layer deep, conductive and non chargeable below the first chargeable layer (for which we kept same parameters of the half space of Figure 2-left).

The extreme variability of the few forward responses plotted above in Figures 1–4 prove that generalisation of results based on the analysis of responses associated with a small subset of the model parameters' space can be risky and inappropriate. This realisation lead to the need of more efficient ways to be able to explore more robustly the model-to-data space relationship and thoroughly appreciate the relevance of IP effects on (1D) data. In this effort, we calculate hundreds of thousands of forward responses, varying the combination of Cole–Cole parameters (ρ, m, τ, c), layering and AEM system's specifications. The transients were then analysed to assess quantitatively, the presence of AIP effects in the data. Obviously this can't be achieved through visual inspection of individual transients. For this task we prepared a series of different IP metrics (Table 2). The basic idea of these metrics is to describe the IP content in each transient as a set of scalar values, capturing complementary aspects of the IP effect on transients. Some metrics integrate signal (positive and/or negative), others fit parts of the transients with exponentials; others again flag the time (gate) at which IP voltages peak or change sign, one describes the sensitivity to model parameters. Metrics 1–5 describe the most obvious AIP effects, i.e. the negatives. Notice that metrics 3 and 5 can be system specific, because they depend on number of gates per decade of time. They will not be used for comparisons across systems. Metrics 6–10 represent an effort to capture the more elusive AIP effects associated with slope changes, with or without sign changes. Metric 11 gives a preliminary view into expected recoverability of IP parameters, if one was to invert for them.

Table 2. Types of metrics used to summarise the AIP effects on both synthetic and real data.

Metrics on gate numbers	1	First gate which shows a negative voltage
	2	Gate which shows the maximum negative voltage
	3	Number of gates which show a negative voltage
Metrics on voltages	4	Maximum negative voltage
	5	Sum of negative voltages
	6	Area below the curve (integral of absolute values)
	7	"pure IP response", that is sum of transient's voltages in presence of chargeability – sum of transient's voltages in absence of chargeability
Metrics on slopes	8	Straight line best fitting in a log-log plot – Early times
	9	Straight line best fitting in a log-log plot – Mid times
	10	Straight line best fitting in a log-log plot – Late times
Metric on sensitivity	11	Covariance of the estimation errors (cfr Auken and Christiansen 2004)

These metrics were derived on the 10^5 forward responses previously calculated, grouped and imaged in 3D, as a function of the Cole–Cole parameters combinations. In order to render the results in 3D, some parameters have to be kept fixed in individual plots, but can be varied across plots. Notice that each metric was only derived on parts of the transient resting above expected noise level. The metrics could also be rearranged and shown differently, but these 3D plots provide an unprecedented quantitative graphical description of the subdomains of the model space

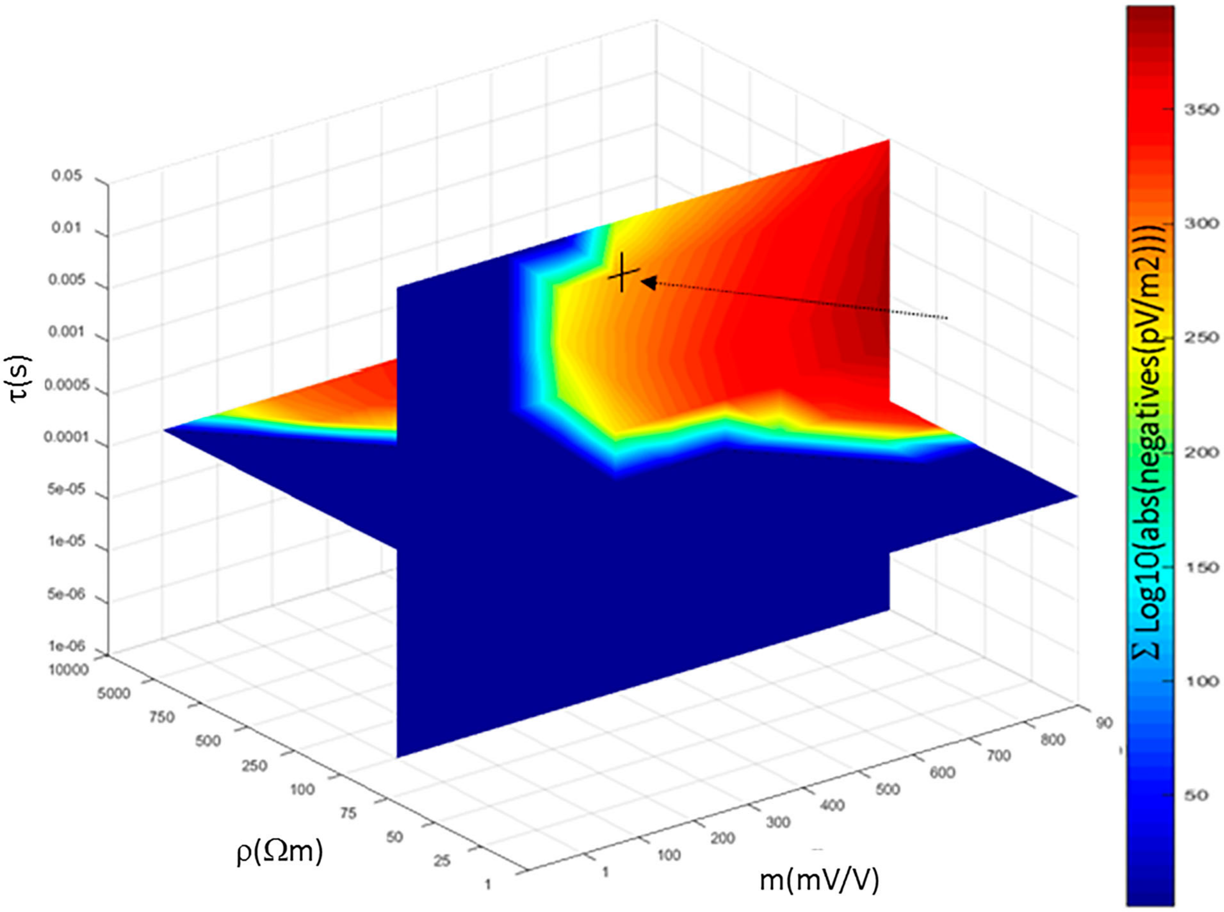

Figure 5. Multidimensional plot showing the combined effects of Cole-Cole parameters (half-spaces, c kept fixed to 0.5) on the VTEM transients. Areas in warm colours represent strong negative anomalies (sum of $\log_{10}$ of negative values). The small cross identifies the individual combination of parameters associated with the transient in Figure 6.

that produce measurable AIP effects. All metrics were inspected in the general study carried out. In the paper we show plots related to all but metric # 3, 6 and 8. We will however use mostly metric #5, because (a) we need a common ground when comparing across the different geological/geophysical scenarios investigated, (b) there are constraints on number of figures that can be presented, (c) this same metric has been used before in the literature when describing IP effects in AEM surveys (e.g. Hine and Macnae 2016).

When calculating the forward responses, parameters were varied in discrete steps within given ranges ($1\ \Omega\text{m} \le \rho \le 10000\ \Omega\text{m}$, $0\ \text{mV/V} \le m \le 900\ \text{mV/V}$, $0.1 \le c \le 1$, $10^{-6}\ \text{s} \le \tau <= 5{*}10^{-2}\ \text{s}$). The actual discrete values used within these ranges can be read in the axis of the figures throughout the paper. Notice that the ranges used are all individually possible in nature. For example, c can vary from 0.1 of the poorly sorted chargeable sources to $c = 1$ of ice. It is arguable whether these combinations among parameters are all possible in nature. Perhaps given subdomains are more likely to exist than others. However, our present understanding is heavily biased by the type of observations carried out in the past, which usually took place at times (frequencies) different from those in which AEM systems focus. The goal of this paper is exactly to extend the boundaries of the commonly accepted, and we therefore scan the entire domain described above.

Unless otherwise specified, we used a VTEM-like (specifications from 2015) system. In the rest of the paper we will refer to this system simply as VTEM. The forward responses were then contaminated with random multiplicative (5%) and additive noise (1 nV/m^2 at 1 ms) to simulate real survey conditions, the metrics of Table 2 calculated and arranged in the 3D plots. The paper is structured to first assess the effect of different geologies and later of different AEM systems configurations. In Figures 5–8 we focus on responses of homogenous half spaces, in Figures 9–11 those of layered models, for the same AEM system. Figures 12–16 revolve around using different AEM systems, different receiver types and under different conditions (i.e. flying height). Figure 17 deals with the correlation between IP effects in data space and sensitivity to model parameters.

Figure 5 shows the first 3D plot of one of these metrics (i.e. the sum of the negative voltages, metric # 5) of the modelled response for half-spaces with different combinations of Cole–Cole parameters (in this view, c is kept constant to 0.5). The sum of negatives is calculated

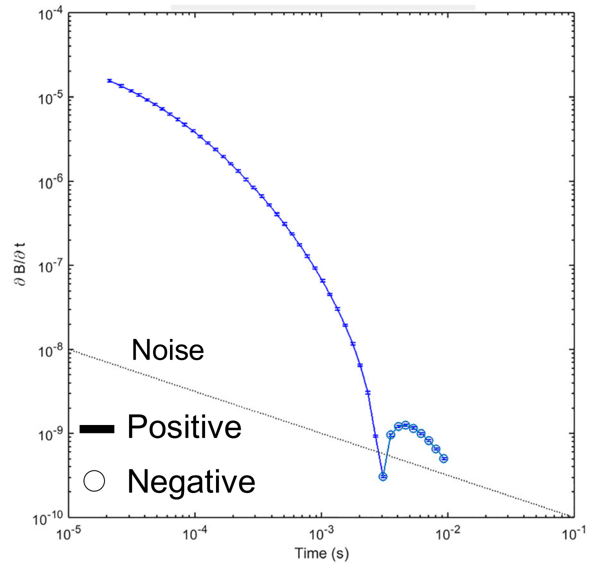

Figure 6. Individual transient (VTEM), associated to a homogeneous half with the following combination of Cole Cole parameters $\rho = 100\ \Omega\text{m}$, m $= 400$ mV/V, $\tau = 10$ ms, c $= 0.5$. The black cross of Figure 5 shows its location in the 3D plot.

on Log10(abs(pV/m^2)). It shows how, in significant parts of this model hyperspace, the Cole–Cole parameters combine to generate strong IP effects which are above the expected noise-levels, hence are detectable under normal survey conditions.

In order to better illustrate the meaning and usefulness of these 3D Plots, we show in Figure 6 the individual transient associated with the point shown in black in Figure 5. It corresponds to a specific combinations of Cole Cole models ($\rho = 100\ \Omega$m, m $= 400$ mV/V, $\tau = 10^{-2}$ s, $c = 0.5$), resulting in the significant negatives shown in both the transient of Figure 6 and in the 3D metric plot of Figure 5. The latter, though, captures how the sum of negative signatures develop in the proximity of that specific combination. For example, it will increase monotonically with *m*, as expected, but first increase and then decrease again as we lower τ, due to limited range of t that can return AIP effects discussed above.

The 3D plots can be inspected at leisure along the fourth dimension, changing the parameter that is kept fixed, and/or its value, and "combing" the 3D spaces. For example, Figure 7 elaborates further on the effect of different background geologies on the sum of negatives (metric # 5), associated with half space resistivity increase.

So far we have shown only metric #5 (the sum of negatives). Figure 8 displays 3D plots of 6 different metrics (metrics # 1,2,4,5,9,10 in A, B, C, D E, F respectively) for another homogenous half space. Specifically, they show: in A and B the number of the gate in the transient with respectively highest negative value and first negative value, in C the value of the maximum of the negative voltage (Log10(V)), in D the sum of the negatives (Log10(abs(pV/m^2))), in *E* and *F* the coefficient of the best fitting of the Mid and Late times portion of the transients respectively. All colorscales are designed to show with warm colours the effects commonly associated to IP in the AEM data (i.e. negatives and/or excessively fast decays).

Figure 8 shows how these metrics have a degree of correlation among themselves, as obvious, but also display different dependence to model parameters' variability. For example, the number of the first negative gate (metric #1) varies more gradually with m than the number of the gate with the maximum negative (metric #2). Unsurprisingly, the rate of decay of the later part of the transient, captured in Figure 8 *F*, depends almost as much on resistivity and on chargeability. This should be duly taken into account when using transient's rate of

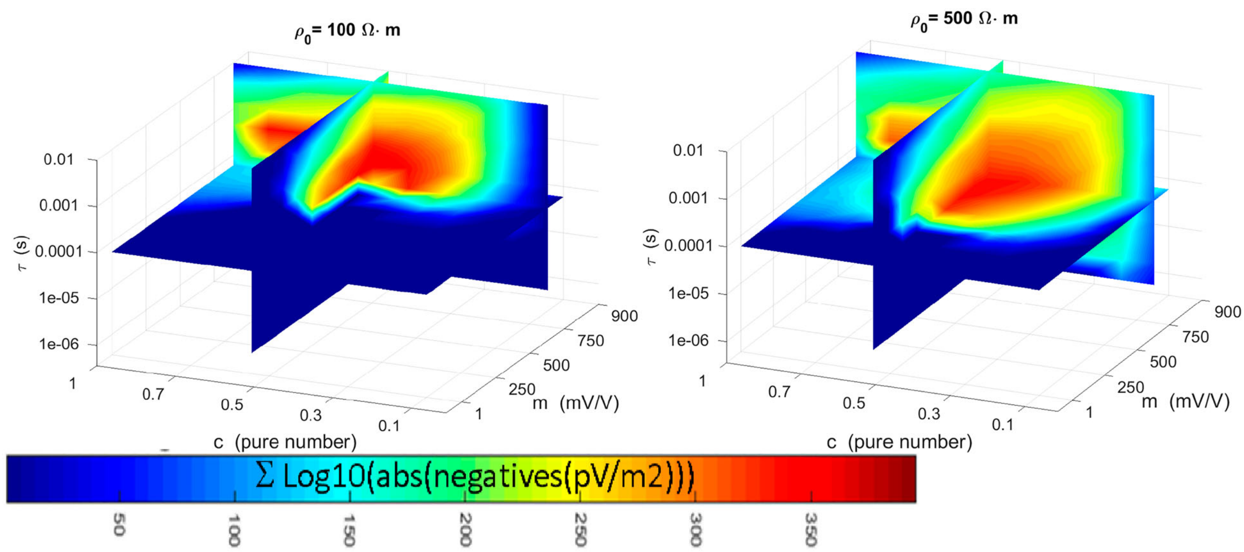

Figure 7. Sum of negative voltages for a homogeneous half-space with different resistivities (100 Ωm left panel, 500 Ωm right panel) from a nominal VTEM system.

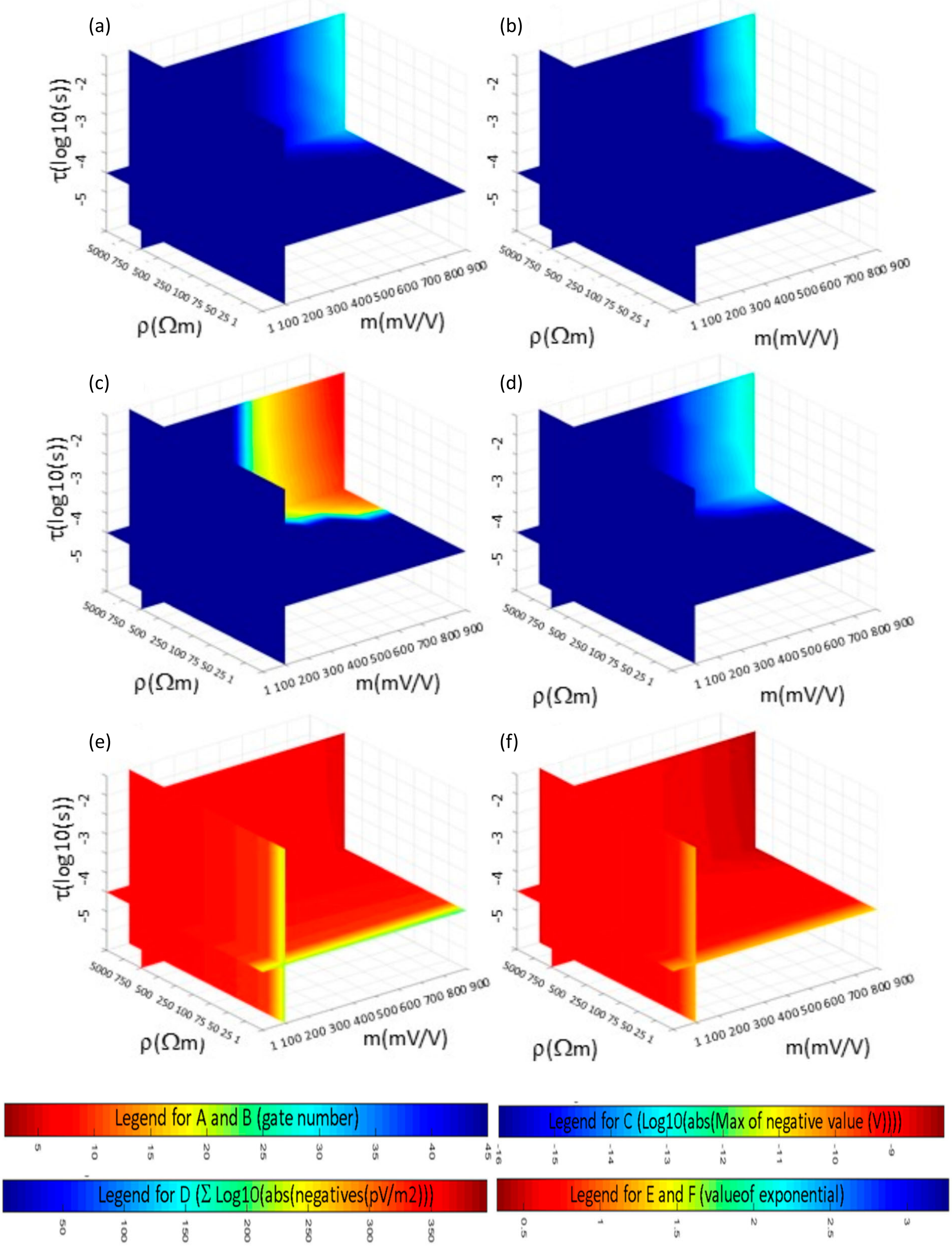

Figure 8. Comparison across 3D plots of different metrics (all VTEM). In all cases $c = 0.2$. (a) Number of gate of maximum negative value; (b) Number of first negative gate; (c) Maximum negative value; (d) Sum of negatives; (e) exponent of best exponential fitting at *Mid times*; (f) exponent of best exponential fitting at *Late times*.

decay for direct interpretation of conductive anomalies, as some times done in mineral exploration.

Combining observations from Figures 5, 7 and 8 allow concluding that, the greater is the resistivity of the half-space, the more spread out are the AIP effects on the data. This is due to the fact that the greater the resistivity the faster the decay of the pure EM current, which makes it easier for the IP currents to overcome the pure EM one. Of course, as the halfspace' resisitivity increases, the overall signal level drops, and the overall

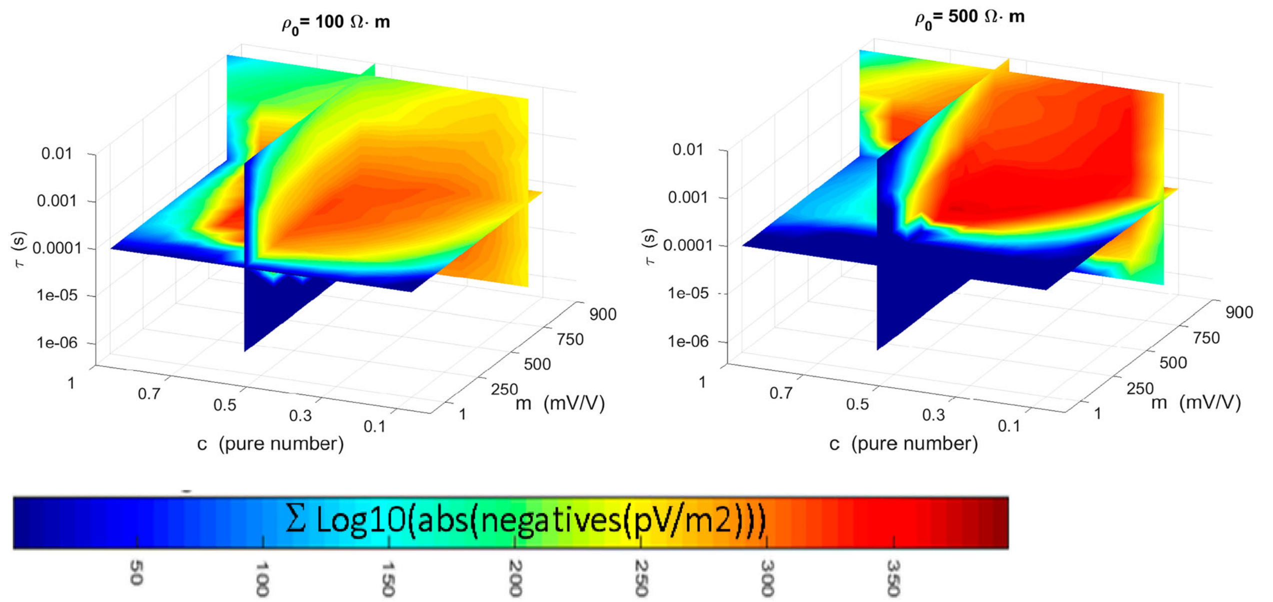

Figure 9. Sum of negative voltages (VTEM) for a two layers half-space, chargeable overburden and resistive (1000 Ωm) bedrock. Resistivity of first layer is 100 Ωm in top panel, 500 Ωm in bottom panel, its thickness 20 m.

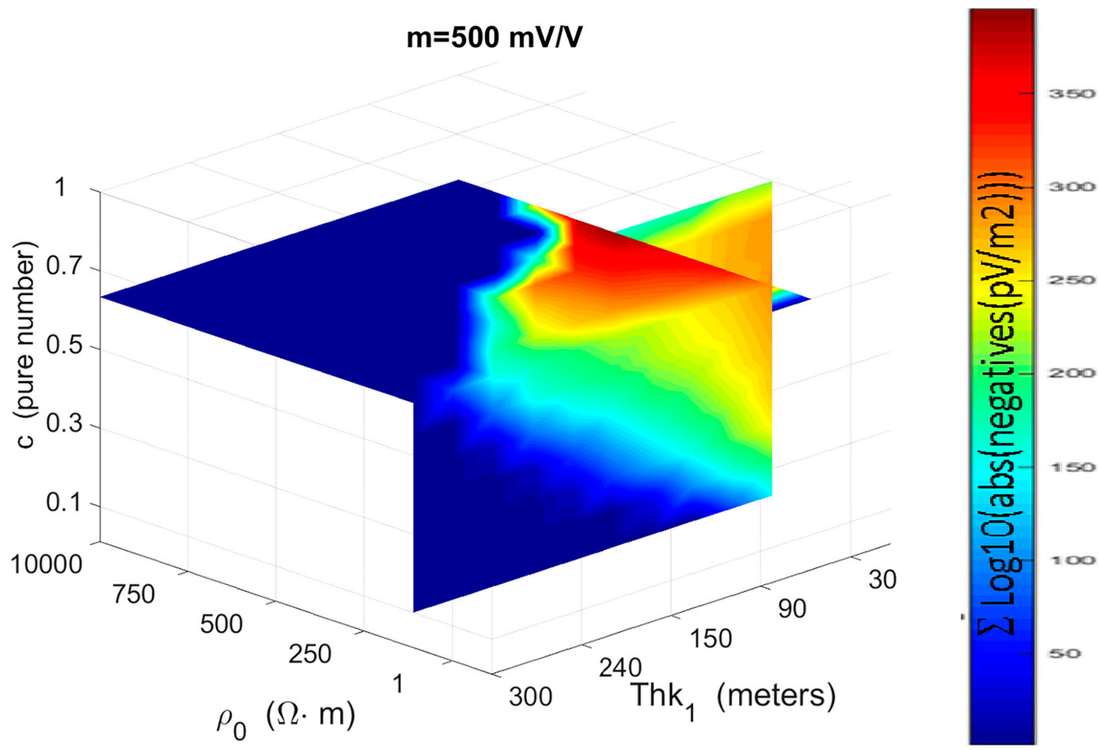

Figure 10. Sum of negative voltages (VTEM) for a three layer model, as a function of electrical properties of second layer (its m = 500 mV/V and $\tau = 10^{-3}$ s are kept constant), and of thickness of first layer. The first and last layers are resistive and non chargeable.

response can drown into noise. Also, as expected, the greater is the chargeability, the more spread out are the IP effects on the data. On the other hand, neither c nor τ have monotonic effects on the AIP effects. This is to be expected for at least 2 reasons: (1) both c and τ have very large and sudden effects on transient's shapes, (2) being directly linked to the phase lag in the Cole Cole model, their effect on measured data interacts strongly with the limited frequency component of the signal measured by AEM. More general findings, arose from the thorough inspection of other 3D Plots for the "simple" half space case study.

As mentioned above, it was soon evident (Figure 4) that layering (vertical variations) of electrical properties may have large impacts on the IP effects. Therefore, after the 3D plots of homogeneous half-space, we moved to a two layers half-space made up of a chargeable overburden 20 meters thick and a highly resistive

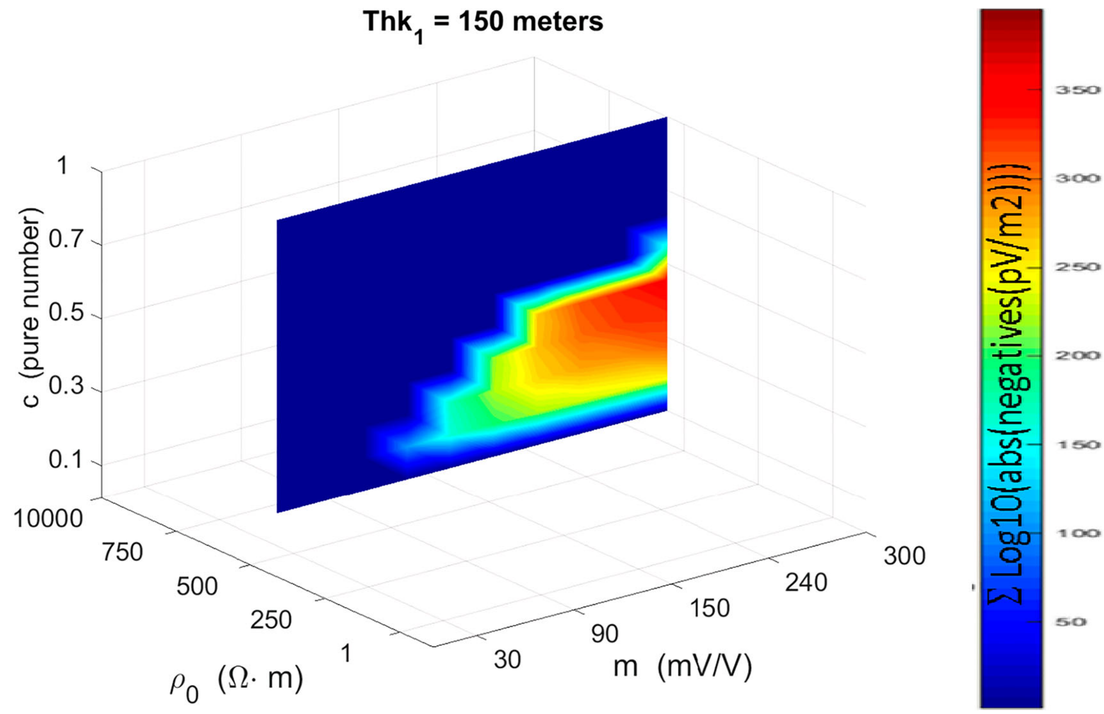

Figure 11. Sum of negative voltages (VTEM) for a three layer model, as a function of electrical properties of second layer, buried at depth of 150 m, chargeable ($\tau = 10^{-3}$ s). The first and last layers are resistive and non chargeable.

bedrock (1,000 Ohm.m). Such scenario is perhaps more frequent than commonly realised. Examples comprise weathered regolith or permafrost, thin artic lakes' bottom sediments, alteration horizons, all above fresh resistive basement rock. We show in Figure 9 using again metric # 5, that the presence of a resistive bedrock has a huge influence on the intensity of the IP effects in the data, increasing it if compared with the homogeneous half-space of Figure 7 (same colorscale). This is because the first chargeable layer "traps" the IP current in the near surface and the highly resistive bedrock quickly dampens the pure EM response. The total measured response is therefore due, to a large degree, to the IP currents only. Increasing chargeability of the first layer always increases IP effects. Once more, c and τ give display more complex relationships.

It is also instructive to compare Figure 9 with Figure 7: not only does the 2 layer model, at a given chargeability value, show much higher sum of negatives with respect to the half space case. It also reports higher sum of negatives for lower chargeabilities than the half space. E.g. a chargeable cover of 100 mV/V, over resistive basement, often creates a sum of negatives of $\sim$300, whereas the homogeneous half space rarely causes sum of negatives above 200, even when its chargeability is 250 mV/V. This is due to the fast shifting balance between contributions from the pure EM and pure IP components to the total response measured (as illustrated in Figure 1). This proves that assessing IP only in the data space may give a very erroneous impression on the actual value of chargeability in the subsurface, and the location (depth) of its source. Recognition of similar effects allows more complete understanding of the very complex relationship data-models in presence of AIP, which can then lead to proper strategies in its analysis.

The last aspect of layering analysed in this paper goes towards better understanding of the depth to which chargeable layers produce measurable AIP effects (Figure 10, metric # 5).

We used a 3 layer model, with the first and last being resistive (1000 Ωm) and non chargeable, while the second was conductive, chargeable ($m = 500$ mV/V, $\tau = 10^{-3}$ s) and 30 m thick. The thickness of the non chargeable cover has large impact on the amount of obvious IP effects in the data. Their relationship is always inverse, but modulated by the other parameters. Figure 10 also shows to that this chargeable layer can produce readily measurable AIP (negatives) effects, even if buried at considerable depths ($>$ 200 m). Notice also how there is a domain of the Cole Cole model space in which metric # 5 due to the buried chargeable layer (Figure 10) is larger than metric # 5 from the chargeable layer at surface (Figure 9). No general relation between depth of chargeable layer and magnitude of AIP effects (e.g. metric # 5) can be drawn.

The effect of varying electrical properties of the chargeable layer ($\tau = 10^{-3}$ kept constant) when buried at constant depth of 150 m are shown in Figure 11 (metric # 5). It proves that, in this range of τ, even moderate chargeabilities can create AIP from at least 150 m of depth.

Our approach can also be useful also to compare extensively the behaviour of different AEM systems. The 3D plot in Figure 12 shows the how much two different

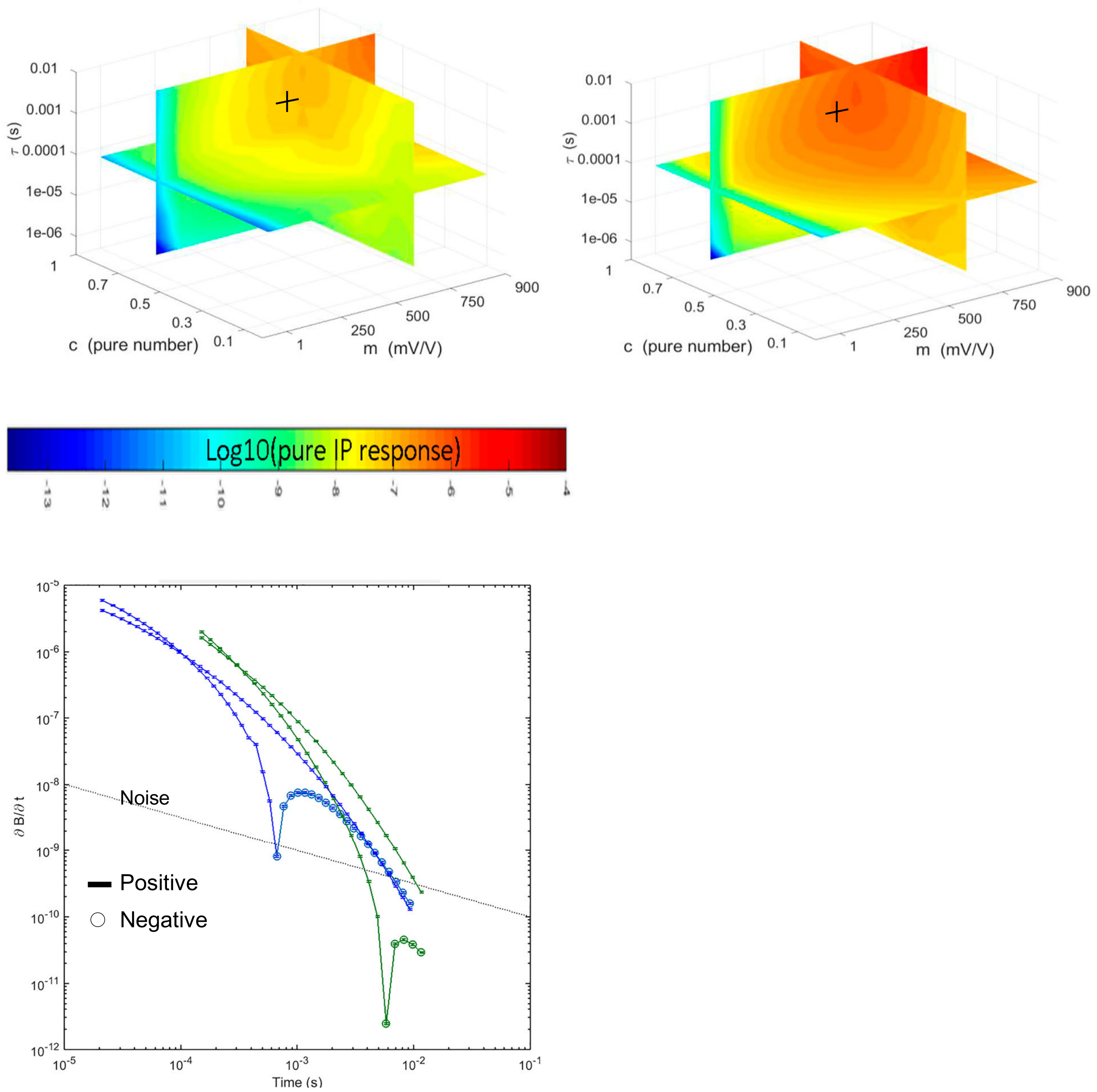

Figure 12. Top: Comparison between sum of voltages generated by the pure IP only current for a homogeneous half-space surveyed with a HeliTEM system (left) and VTEM (right). Bottom: For comparison, individual transients (VTEM blue, HeliTEM green) associated with homogeneous halfspace with the following combination of Cole Cole parameters: $\rho = 200\ \Omega$m, $\tau = 1$ ms, c $= 0.5$, m $= 400$ mV/V, compared to the response of the non chargeable half space of $\rho = 200\ \Omega$m. Their differences render the "pure IP effect". The black cross in the 3D plot shows the location of the combinations associated with these transients in the 3D plot.

EM systems – in this case VTEM and HeliTEM – can differ from each other in their AIP signature over homogeneous half spaces (constant $\rho = 200\ \Omega$m). This time we use metric # 7, aimed at isolating the "pure IP response", separated from the EM response. It is obtained calculating first all forward responses without chargeability, then with chargeability, subtracting them and adding up the (Log10) voltages along the resulting transients. For added clarity, the insert in Figure 12 shows couples of transients (VTEM and HeliTEM, with and without IP), for the point of the 3D space shown by the black cross. The "pure IP" response is larger for VTEM, at least for this specific parameter combination. The 3D plot proves this to be a general result. The duration of ramp down of the two systems is similar ($\sim$2 ms), so it can't be the main reason for the difference. In this case, VTEM excites broader IP anomalies thanks to the wider range of frequencies contained in its trapezoid waveform with respect to those originating from the half sinusoid of the HeliTEM.

Figure 13 explores in more detail the response of the Helitem system, using metrics 1,2,3,5 over the same 2 layer model of Figure 9. As previously discussed for Figure 8, the diverse metrics are complementary in describing the IP effect. Some of the anomalies peaks are is neighbouring subdomains, although not coincident, while others rest in rather different ones. Once again, settling on a particular metric for a real dataset

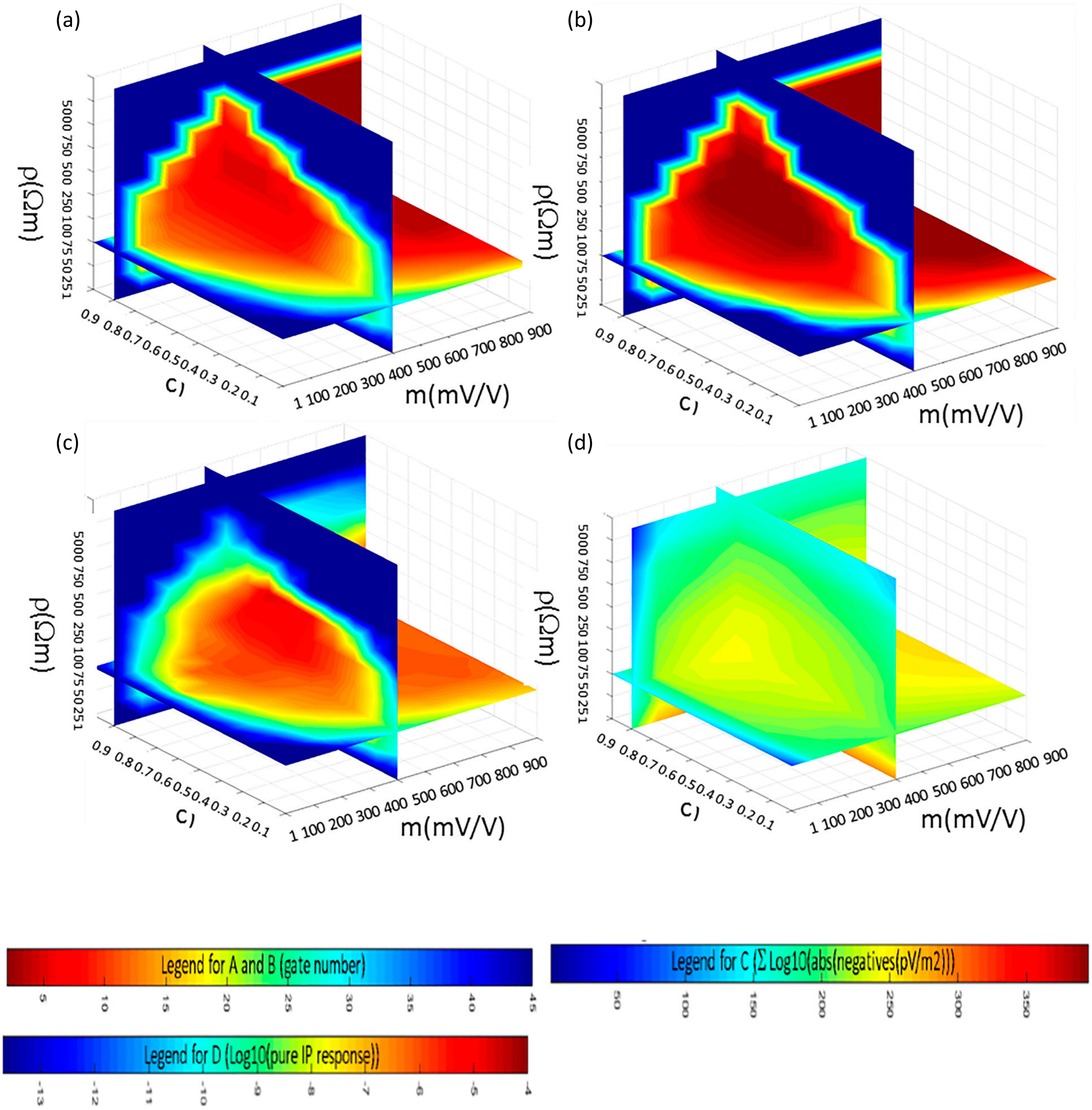

Figure 13. Comparison across 3D plots of different metrics (HeliTEM). In all cases $c = 0.5$. (a) Number of gate of maximum negative value; (b) Number of first negative gate; (c) Number of negative gates; (d) Sum of negatives.

returns only very partial insight into the actual magnitude of the chargeability target and, e.g. its source type (which is loosely linked to τ and c).

We then moved to assessing the effect of lowering base frequency of the AEM system, a goal that many contactors are actively pursuing (a 6.25 Hz version of a "standard" system is presently on the market). For instance, we can compare in Figure 14 (back to metric # 5) how much IP effects are recorded using a VTEM-like system with a base frequency at 25 Hz with the same system at 12.5 Hz. Using a 12.5 Hz system the sum of negative voltages increases compared to the 25 Hz system. The contribution of the IP current to the total signal is far stronger at late-times than at early-times. So, if one wants to record much information as possible about the chargeable bodies, is advisable to use a system with a low base frequency (provided the signal stays above noise level, which may require higher dipole moments and/or quieter receivers).

We also studied how much AIP effects can be better observed recording the B field instead of its derivative. In B field recording the change of sign appears earlier, compared to the same measure in dB/dt. This makes it often possible, in theory, to recover more information about the chargeable bodies. Figure 15 shows the comparison between the B field and the dB/dt using the first gate which shows a negative value (metric # 1). As well known, the B field records the first gate at earlier times. This could make the difference in instances when the IP effects become evident close to the last gate.

Finally, we looked into effect of flight altitude. The 3D plot in Figure 16 uses metric # 5 to show the AIP effects

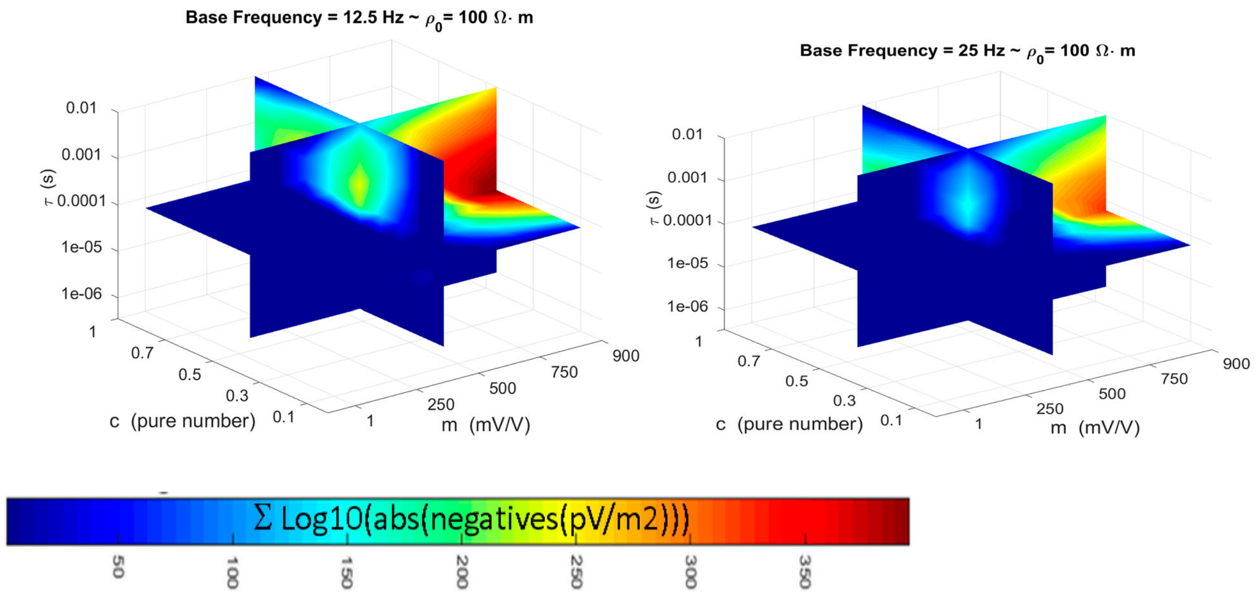

Figure 14. Comparison between sum of negative voltages for a homogeneous half-space surveyed with a VTEM 12.5 Hz (above) and VTEM 25 Hz (below).

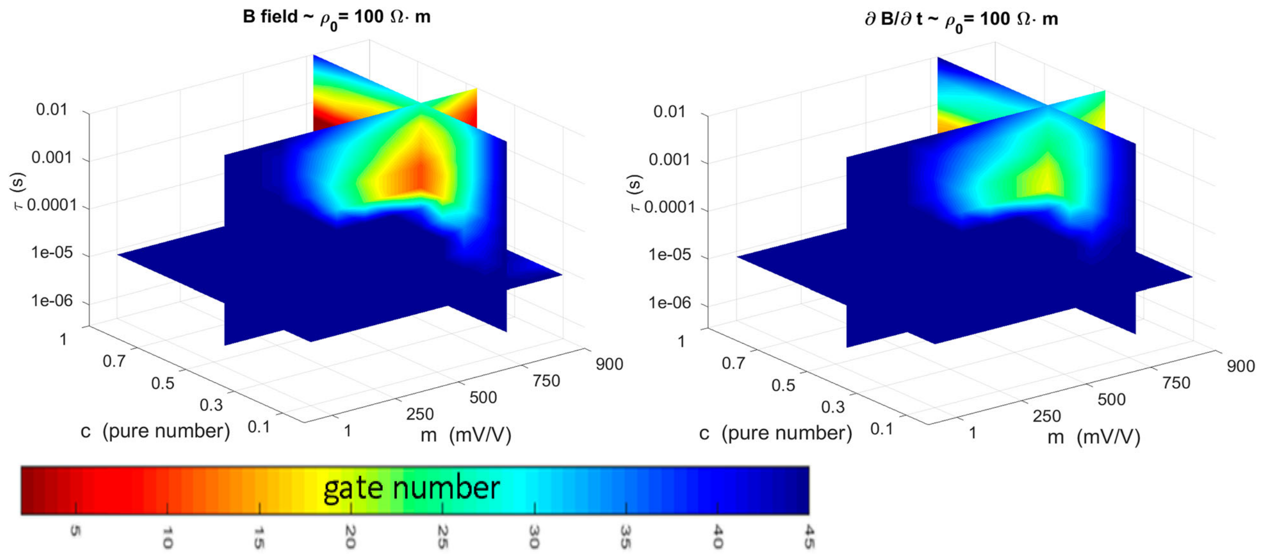

Figure 15. Comparison between the of sum of number of gates having negative voltages for a homogeneous half-space surveyed with a VTEM system B field (above) and dB/dt (below).

(always on Z component) as function of half space Cole Cole parameters (m, c, ρ), at altitudes of 30 and 100 m. The τ parameter was constant (1 ms). Unsurprisingly, the higher flying platforms produce weaker AIP effects. Notice also the large magnitude of the effects of different heights, which calls for accurate measuring of the actual ground clearance of the AEM system's frame.

The approach presented so far maps the AIP effects in data space. But it is important to note that there is no simple univocal direct correlation between the intensity of AIP effects in the data (not limited to their unmistakeable negatives signature) and the potential recoverability of IP parameters. In order to show this, we computed the sensitivity to the four Cole–Cole parameters in homogeneous half spaces' response. The sensitivity, based on the covariance of the estimation errors (Auken and Christiansen 2004), is a measure of how much a given parameter (in this case, Cole Cole's) influences the data. The greater the sensitivity for a certain parameter, the easier to recover it from the data through inversion. Figure 17 shows the correlation between the sum of negative voltages (metric #5) and the corresponding sensitivity (metric #11), for the same 2 layer model of Figure 9 (first layers chargeable, VTEM response). High value of the sum of negative voltages doesn't necessarily correspond to sensitivity highs, and vice versa. This is due to the contribution to the sensitivity calculations coming from the entirety of the transient. This point is particularly relevant, as it proves that assessing IP only in the data space may give a wrong impression not only of where the chargeabilities are actually higher, but also where they stand a chance of getting recovered more robustly through inversion. The same goes for the depth from which AIP effects originate.

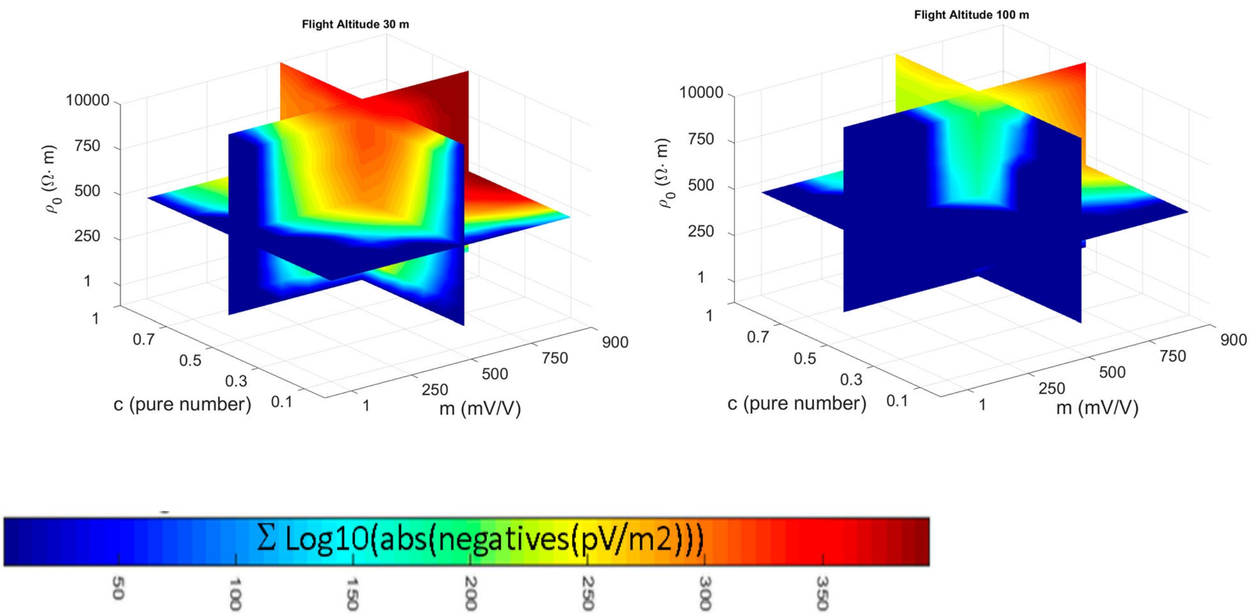

Figure 16. Sum of negative voltages for a homogeneous half-space for different platforms height (30 m left, 100 m right). The τ parameter was constant (1 ms).

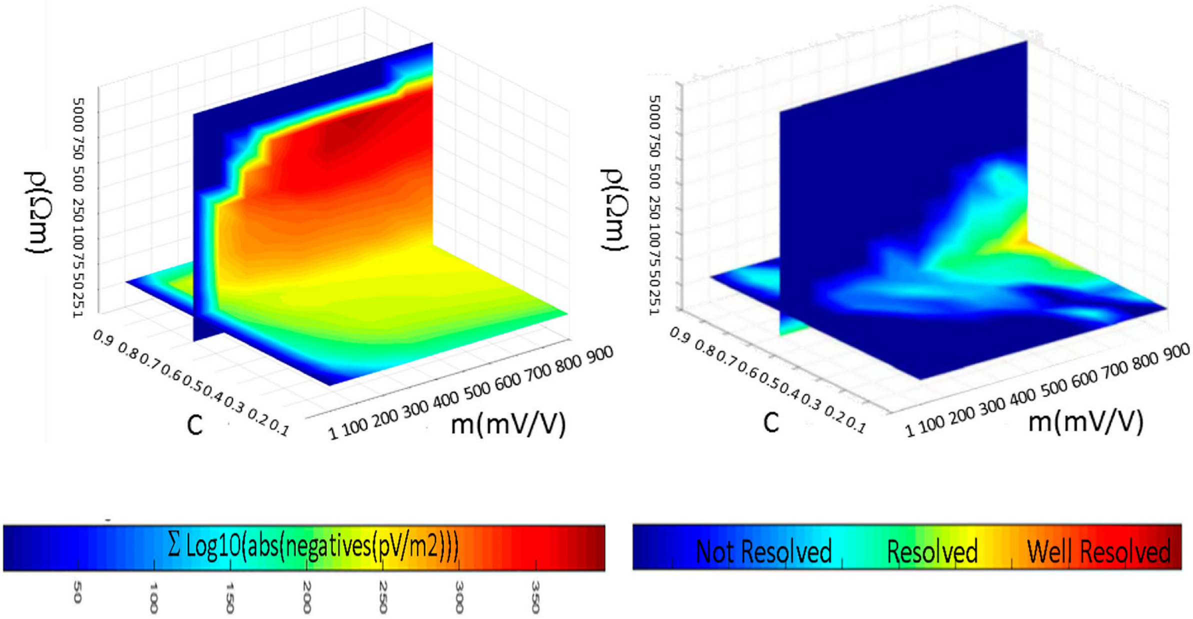

Figure 17. Comparison between sum of negative voltages (above) and the sensitivity on chargeability (below, better resolved parameters in red) for the 2 layered model of Figure 9, for a VTEM system.

The results presented herein describe just a subset of the whole analysis we carried out using the 3D plots of the metrics. Let us summarise here the general findings:

(1) In a homogeneous and chargeable half-space, AIP effects never decrease with increasing resistivity and chargeability, but there are large domains where they are unaffected by their changes;
(2) Vertical layering of electrical properties greatly affects AIP. In a two layers half-space the presence of a resistive bedrock under a chargeable overburden greatly enhances AIP effects. In three layer systems, a chargeable layer (with τ in the range of 10^{-2} s to 10^{-4} s) buried at 300 m overlaying a resistor can return a measurable AIP effect;
(3) There is no direct and general correlation between magnitude of measured AIP effects and depth of the chargeable layers
(4) EM systems having slower turn off time generally excite the chargeable material over a wider range of τ than EM systems having faster turn off time, due to the broader range of τ they excite;
(5) EM systems with lower frequency (e.g. 12.5 Hz) often display higher sensitivity to the Cole–Cole parameters, with the exception of situations where the transient falls into noise before reaching the last gates;

(6) EM systems able to measure the B field instead of its derivative also often display higher sensitivity;
(7) There is no simple direct correlation between the intensity of AIP effects of a certain parameter, its sensitivity and expected recoverability through inversion;
(8) AIP is strongly dependent on flying height.

It is worth stressing that the points above confirm the evidences gathered by the authors in dozens of consulting projects that included full IP modelling of actual AEM datasets, on different systems and in different geologies. The results of the full inversions to models showing the spatial variability of the 4 Cole Cole parameters invariably brought significant surprises and added insight about the subsurface when compared to the preliminary assessments of AIP carried out merely in the data space (e.g. Di Massa et al. 2017; Kaminski and Viezzoli 2017).

As mentioned above, it has been shown before (E.g. Hine and Macnae 2016; Viezzoli, Kaminski, and Fiandaca 2017, 106) how IP affected data that are modelled without taking IP into account will produce artefacts, at times very severe, in the resulting resistivity models. A typical example is the underestimation of bedrock's conductivity and depth. In other cases, even bedrock conductors can disappear. The findings listed above are therefore relevant also when the only goal of the AEM survey is to model resistivity.

Conclusions

The results presented herein offer a solid base for better understanding and recognition of the range of AEM data (both existing and yet to be acquired) affected by IP. They are relevant for AIP processing, inversion and further interpretation.

Detailed analysis of 10^5 FWD responses (different combinations of Cole Cole parameters and layering-layered earth approach) prove that measurable IP effects (in the range of τ centred between 10^{-2} and 10^{-4}) in AEM:

(1) are to be expected under many conditions, that is in virtually all cases where a chargeable layer overlays a resistive layer,
(2) can originate from considerable depths (in presence of a resistive layer below the chargeable layer),
(3) can produce rather unpredictable signatures, e.g. the non monotonic effect of τ,
(4) are hugely affected by layering, thanks to the sudden changes that can take place in relative contribution of "IP" versus "EM" currents to the total measured response,
(5) are rather dependent on actual system specifications, especially their waveforms that can either enhance or reduce them,
(6) are, in presence of shallow chargeable layers, very dependent on flying height,
(7) have a magnitude that can't be generally correlated with actual depth of the chargeable source, nor its magnitude

As a consequence, robust assessment of AEM data should routinely contain investigation about possible presence of AIP effects (this goes beyond presence of negatives). Furthermore, keeping in mind the potential artefacts that can arise from ignoring AIP, robust modelling of AEM data that could contain even small amounts of AIP effects should entail full IP inversion.

Acknowledgments

This project has received funding from the European Union's Horizon 2020 research and innovation programme under grant agreement No 776487.

Disclosure statement

No potential conflict of interest was reported by the authors.

Funding

This project has received funding from the European Union's Horizon 2020 research and innovation programme under grant agreement No 776487.

References

Auken, E., and A.V. Christiansen. 2004. Layered and laterally constrained 2D inversion of resistivity data. *Geophysics* 69: 752–61.
Chen, T., G. Hodges, and A. Smiarowski. 2015. Extracting subtle IP responses from airborne time domain electromagnetics data. SEG, New Orleans Annual Meeting, Extended Abstract.
Di Massa, D., M. Fedi, G. Florio, A. Vitale, A. Viezzoli, and V. Kaminski. 2017. Joint interpretation of AEM and aeromagnetic data acquired over the Drybones kimberlite, NWT (Canada).
Fiandaca, G., E. Auken, A. Gazoty, and A.V. Christiansen. 2012. Time-domain-induced polarization: Full-decay forward modeling and 1D laterally constrained inversion of cole-cole parameters. *Geophysics* 77, no. 3: E213–25.
Flis, M., G.A. Newman, and G.W. Hohmann. 1989. Induced-polarization effects in time-domain electromagnetic measurements. *Geophysics* 54: 514–23.
Hine, K., and J. Macnae. 2016. Comparing induced polarization responses from airborne inductive and galvanic ground systems: Lewis Ponds, New South Wales. *Geophysics* 81, no. 6: B179–88.
Kaminski, V., and A. Viezzoli. 2017. Modeling induced polarization effects in helicopter time-domain electromagnetic data: Field case studies. *Geophysics* 82, no. 2: B49–61.
Kang, S., D. Fournier, and D. Oldenburg. 2017. Inversion of airborne geophysics over the DO-27/DO-18 kimberlites – Part 3: Induced polarization. *Interpretation* 5: T327–40.
Kratzer, T., and J.C. Macnae. 2012. Induced polarization in airborne EM. *Geophysics* 77: E317–27.

Macnae, J. 2016. Quantitative estimation of intrinsic induced polarization and superparamagnetic parameters from airborne electromagnetic data. *Geophysics* 81, no. 6: E433–46.

Macnae, J. 2017. Towards and extremely low frequency AEM system with AIP capability: BIPTEM. SAGA. 15th Biennial Conference & Exhibition, September 10–13, 2017, Cape Town.

Oldenburg, D.W., and S. Kang. 2015. Recovering IP information in airborne-time domain electromagnetic data. 24th ASEG-PESA meeting – Perth, Extended Abstract.

Smith, R.S. 1989. On induced polarization effects in time domain electromagnetic measurements, discussion. *Geophysics* 54: 514–23.

Smith, R.S., and G.F. West. 1988. Inductive interaction between polarizable conductors: An explanation of a negative coincident-loop transient electromagnetic response. *Geophysics* 53: 677–90.

Smith, R.S., and J. Klein. 1996. A special circumstance of airborne induced-polarization measurements. *Geophysics* 61: 66–73.

Viezzoli, A., V. Kaminski, and G. Fiandaca. 2017. Modeling induced polarization effects in helicopter time domain electromagnetic data: Synthetic case studies. *Geophysics* 82, no. 2: E31–50.